Research Article | Vol. 13, No. 5 / 1 May 2022 / Biomedical Optics Express 3131
Biomedical Optics EXPRESS

Millimeter waves alter DNA secondary structures and modulate the transcriptome in human fibroblasts

NICHOLAS B. LAWLER,[1,2] CAMERON W. EVANS,[2] SERGII ROMANENKO,[3] NUTAN CHAUDHARI,[2] MARK FEAR,[4] FIONA WOOD,[5] NICOLE M. SMITH,[2,6] VINCENT P. WALLACE,[1,7] AND K. SWAMINATHAN IYER[2,8]

[1]*Department of Physics, The University of Western Australia, Perth, WA 6009, Australia*
[2]*School of Molecular Sciences, The University of Western Australia, Perth, WA 6009, Australia*
[3]*Department of Sensory Signaling, O.O. Bogomolets Institute of Physiology, National Academy of Sciences of Ukraine, Kyiv, 01601, Ukraine*
[4]*Burn Injury Research Unit, School of Biomedical Sciences, University of Western Australia, Perth, WA 6009, Australia*
[5]*Fiona Stanley and Princess Margaret Hospitals, Burns Service of Western Australia, Perth, WA, Australia*
[6]*nicole.smith@uwa.edu.au*
[7]*vincent.wallace@uwa.edu.au*
[8]*swaminatha.iyer@uwa.edu.au*

Abstract: As millimetre wave (MMW) frequencies of the electromagnetic spectrum are increasingly adopted in modern technologies such as mobile communications and networking, characterising the biological effects is critical in determining safe exposure levels. We study the exposure of primary human dermal fibroblasts to MMWs, finding MMWs trigger genomic and transcriptomic alterations. In particular, repeated 60 GHz, 2.6 mW cm^{-2}, 46.8 J cm^{-2} d^{-1} MMW doses induce a unique physiological response after 2 and 4 days exposure. We show that high dose MMWs induce simultaneous non-thermal alterations to the transcriptome and DNA structural dynamics, including formation of G-quadruplex and i-motif secondary structures, but not DNA damage.

1. Introduction

Millimeter waves, electromagnetic radiation with frequencies of 30 to 300 GHz and 1–10 mm wavelengths, are of growing biological interest as they become increasingly prevalent in our lives due to their implementation in emerging technologies utilising ultra-fast data transportation. These frequencies are attractive for data transmission as they deliver ultra-fast data rates, a very low latency, and significantly improved spectral efficiency over existing technologies [1,2]. This has prompted rapid adoption in common technologies including mobile communications and networking [1,3–5], and security screening [6].

The atmospheric attenuation of MMWs is highly frequency-dependent; strong absorption by water and oxygen results in a maximal attenuation of 16 dB km^{-1} at 60 GHz [7–9]. The lack of planetary sources and attenuation of astronomical radiation by the atmosphere has historically limited human exposure to MMWs, and the biological effects are not well characterised [10,11]. Recently, it has been demonstrated that MMWs can induce numerous effects on a cellular level, including to neuronal action potentials [12], membrane properties [13,14], and gene expression [15–19]. Initially, modified gene expression was attributed to the heat shock response of cells to the heating associated with absorption of the MMWs, however it has been shown these

#458478 https://doi.org/10.1364/BOE.458478
Journal © 2022 Received 16 Mar 2022; revised 14 Apr 2022; accepted 14 Apr 2022; published 28 Apr 2022

Biomedical Optics EXPRESS

modifications are not solely due to thermal effects and the interaction mechanisms driving this altered transcriptomic profile remain an area of interest [15].

The high water content of human tissue means that this non-ionising radiation has a penetration depth less than 1 mm (typically on the order of hundreds of micrometres) and is absorbed by the epidermal and dermal layers of skin [11,20,21]. As key cellular components of the dermal layer of the skin, fibroblasts exhibit a characteristic cellular response to stress, which is accompanied by increased production and deposition of extracellular collagen. This has been observed in response to a range of stress initiators, including trauma, infections, radiotherapy, chemotherapy, alcohol exposure, and toxins [22].

In this work we explored the effects of repeated 60 GHz MMW exposures at 2.6 mW cm^{-2}, 46.8 J cm^{-2} d^{-1} doses for 2 and 4 days, on primary human fibroblasts. The delivered dose is at higher power densities than the limits of 2 mW cm^{-2} for 6 min and 1 mW cm^{-2} for 30 min recommended by the International Commission on Non-ionising Radiation Protection [23,24]. It is important to understand the effects of high doses in determining safe exposure levels and thresholds. We observe modifications at the genomic, transcriptomic, and cellular levels via RNA-seq, qPCR and immunocytochemistry. From these results we identified altered biological pathways associated with G-quadruplex (G4) and i-motif (iM) DNA.

G4s and iMs are non-canonical four-stranded secondary structures that form within certain guanine- and cytosine-rich DNA sequences, respectively, and are over-represented in regulatory regions of the human genome. These structures contribute to regulation of transcription, recombination, and replication processes [25,26]. We examined the formation of G4s and iMs, and their association with genes altered by MMW exposure *via* immunocytochemistry and predictive algorithms. Our results reveal high dose MMWs induce alterations at multiple levels of the transcription and translation processes, with changes to protein production, gene expression, and DNA structures, representing unique interactions of MMWs with biological material at the cellular level.

2. Materials and methods

2.1. Experimental model and subject details

All human tissue samples were collected after patients had signed informed consent and with ethical approval from the human ethics committees at the University of Western Australia or South Metropolitan Health Service and in accordance with the NHMRC National Statement on Ethical Conduct in Human Research. Human primary skin fibroblasts were collected from healthy individuals undergoing elective surgery resulting in discarded skin tissue (Normal fibroblasts). Fibroblasts were grown in culture using a standard explant protocol [27]. Cells were subsequently cultured in DMEM-Glutamax (Gibco, 10569-010) supplemented with 10% v/v fetal bovine serum (FBS) (Gibco, 16000-044) and 100 U/mL penicillin/streptomycin (Gibco, 15140-122). Cells were maintained in log growth phase at 37 °C, 5% CO_2 in a humidified incubator and passaged at 80-90% confluency with 1x TrypLE Express (Gibco, 12604-013). Cell culture medium was replaced every 2 days, and experiments conducted on cells between passages P4-P7.

2.2. MMW setup

The MMW generation system consisted of a microwave tuned oscillator source for 8–20 GHz (YIG tuned oscillator SAO 002, Virginia Diodes Inc. Charlottesville, VA), frequency multiplier/power amplifier chain stage (WR12AMC-HP, Virginia Diodes Inc. Charlottesville, VA) delivering a tunable signal in the range 60–90 GHz and output power 20 dB m. Power levels were controlled using internal attenuators. For these experiments, we tuned the frequency to 60 GHz and used the maximal output power (100 mW).

Biomedical Optics EXPRESS

2.3. MMW stimulation

Cells were prepared similarly for both immunofluorescence and RNA experiments. Cells were plated at 250,000 cells mL^{-1} in 6-well plates (on coverslips for immunocytochemistry experiments) in normal growth media and maintained at 37 °C, 5% CO_2 for 16 h to reach confluency. After 16 h the media was replaced with low serum crowding media containing DMEM-Glutamax (Gibco, 10569-010) with 0.5% v/v FBS, 100 µM L-ascorbic acid (Ajax Finechem, AJA79), 37.5 mg mL^{-1} Ficoll PM70 (Sigma, F2878) and 25 mg mL^{-1} Ficoll 400 (Sigma, 2637) [28]. For exposure of the fibroblasts, the 6-well plates were suspended less than 2 mm above the WR12 waveguide and raster scanned through the 100 mW MMW beam, with the beam passing through the plastic base of the well to irradiate the cells, resulting in an average power density of 2.6 mW cm^{-2}. The raster scan covered 4 wells of the 6-well plate, a total of 38.48 cm^2 (9.62 cm^2 per well), by scanning through each well completely before moving to the next and repeating at the end of the cycle. The scanning is continuous at 12.8 mm s^{-1} in the *x*-direction and 1.5 mm steps in the *y*-direction, for a period of 362 s for a full cycle. The plate was positioned 2 mm above the waveguide (3.09×1.54 mm aperture). The average power was determined from the beam power and total exposed area, and dose calculated for the 5 h exposure period.

Cells were exposed to MMWs for 5 h per day, 46.8 J cm^{-2} d^{-1} doses (energy delivered by the MMW beam per unit area each day), for 4 days (187.2 J cm^{-2} total for collagen, BG4, iMab and γH2AX immunofluorescence), or 2 days (93.6 J cm^{-2} total for RNA-seq and qPCR). Control samples were subject to identical conditions and raster scanned without MMWs. Transforming growth factor beta (TGF-β) treated samples were subject to identical conditions with 5 ng/mL TGF-β (R&D Systems, RDS240B002) added to the low serum crowding media and raster scanned without MMWs. During the 5 h/day period of raster scanning the control, MMW and TGF-β treated cells were maintained at room temperature (25 °C) and at atmospheric CO_2 levels, and were returned to 37 °C, 5% CO_2 after each exposure. The control condition was compared with growth control samples that were maintained in culture media and at 37 °C, 5% CO_2 for the same time period.

2.4. Extracellular collagen immunofluorescence

Cells were washed twice with Fluorobrite (Gibco, A1896701) and blocked with 3% bovine serum albumin (BSA) (Sigma, A9418) for 30 min at room temperature then incubated for 90 min at 37°C with mouse monoclonal anti-collagen antibody (Sigma, C2456) (diluted 1:1000 in 3% BSA in Fluorobrite). Cells were washed twice with Fluorobrite and fixed for 15 min with 4% paraformaldehyde (PFA) (Scharlau, PA00950500) in phosphate buffered saline (PBS). The cells were washed twice with PBS and incubated at 37 °C for 30 min with secondary antibody solution of donkey anti-mouse Alexa Fluor 488 (Abcam, ab150105) (4 µg/mL) and Hoechst 34580 (Sigma-Aldrich, 63493) (1 µg/mL) in PBS. Coverslips were washed twice with PBS and mounted on glass microscope slides (Corning) with Fluoromount-G mounting media (Invitrogen, 00-4958-02).

2.5. BG4 immunofluorescence

G4 structures in the nuclei were targeted with the structure-specific FLAG-tagged scFv-BG4 antibody (MABE917, Millipore).

To prevent the staining of cytoplasmic G4s, cells were prefixed with 2% w/v PFA in PBS for 2 min before incubation for 15 min at room temperature with cytoplasm removal buffer (20 mM HEPES-KOH, 20 mM NaCl, 5 mM $MgCl_2$, 300 mM sucrose, 0.5% v/v NP-40 Surfact-Amps Detergent Solution (Thermo Fisher, 85124), pH 7.9 in PBS. Coverslips were briefly incubated with 0.1% v/v Triton X-100 (Sigma-Aldrich, T8787) in PBS and PBS before being fixed for 20 min with 2% w/v PFA in PBS. Cells were washed twice with PBS and permeabilized with

Biomedical Optics EXPRESS

0.1% v/v Triton X-100 in PBS for 10 min, washed twice with PBS, and blocked with 2% w/v BSA, 1% w/v skim milk in PBS at 4 °C overnight. Coverslips were inverted on 50 µL drops of FLAG-tagged BG4 antibody (300 nM in 2% w/v BSA in PBS) on parafilm and incubated at 37 °C for 1 h then washed three times with 0.1% v/v Tween 20 (Sigma-Aldrich, P9416) and incubated with rabbit anti-FLAG antibody (Cell Signalling Technology, 2368) (diluted 1:1000 in 2% w/v BSA) for 1 h at 37 °C. Coverslips were washed three times with 0.1% v/v Tween 20 before incubation for 30 min at 37 °C with antibody solution containing goat anti-rabbit Alexa Fluor 594 (ThermoFisher, A11037) (1 µg/mL) and Hoechst 34580 (1 µg/mL) in 2% w/v BSA in PBS. Coverslips were washed thrice with 0.1% v/v Tween 20 and twice with PBS and mounted on glass microscope slides (Fluoromount-G).

2.6. iMab immunofluorescence

DNA i-motifs were targeted with the structure specific FLAG-tagged scFv-iMab antibody [29].

Cells were prefixed with 2% w/v PFA in PBS for 2 min followed by incubation for 15 min at room temperature with cytoplasm removal buffer. The coverslips were briefly incubated with 0.1% v/v Triton X-100 in PBS and PBS before being fixed for 20 mins with 2% w/v PFA in PBS. Cells were washed twice with PBS and permeabilised with 0.1% v/v Triton X-100 for 30 min at 4 °C and washed twice with PBS. The cells were blocked overnight at 4 °C with 2% w/v BSA and 1% w/v skim milk in PBS then incubated overnight at 4 °C with the FLAG-tagged iMab antibody (200 nM in 2% w/v BSA, 1% w/v skim milk in PBS). Coverslips were washed thrice with ice-cold PBS and incubated for 45 mins at room temperature with rabbit anti-FLAG antibody (diluted 1:800 in 2% fish gelatin (Sigma, G7041), 0.5% w/v BSA, 0.1% v/v Tween 20 in PBS). Cells were washed three times with ice-cold PBS and incubated for 45 min at room temperature with goat anti-rabbit Alexa Fluor 594 (5 µg/mL) and Hoechst 34580 (1 µg/mL) in 2% fish gelatin, 0.5% w/v BSA, 0.1% v/v Tween 20 in PBS. Coverslips were washed twice with 0.1% Tween 20 and rinsed with PBS then mounted on glass microscope slides with Fluoromount-G mounting media.

2.7. γH2AX immunofluorescence

Cells were prefixed with 2% w/v PFA in PBS for 2 min, incubated with cytoplasm removal buffer (20 mM HEPES-KOH, 20 mM NaCl, 5 mM $MgCl_2$, 300 mM sucrose, 0.5% v/v NP-40 Surfact-Amps Detergent Solution (Thermo Fisher, 85124), pH 7.9 in PBS) for 15 min at room temperature then washed with 0.1% Triton X-100 in PBS and PBS. The cells were fixed with 2% w/v PFA in PBS for 20 min and washed twice with PBS then permeabilised with 0.1% v/v Triton X-100 for 10 min at room temperature. The cells were washed twice with PBS and blocked with 3% w/v BSA in PBS for 1 h at room temperature then washed three times with PBS and incubated for 2 h at room temperature with rabbit anti-γH2AX antibody (Abcam, ab11174) diluted 1:500 in 1% w/v BSA in PBS. Coverslips were then washed three times with PBS and incubated for 1 h at room temperature with goat anti-rabbit Alexa Fluor 594 (diluted 1:1000) and Hoechst 34580 (1 µg/mL) diluted in 1% w/v BSA in PBS. Coverslips were washed with 0.1% v/v Tween 20 and rinsed with PBS then mounted on glass microscope slides with Fluoromount-G mounting media.

2.8. Imaging and quantification

Imaging of the immunocytochemistry samples was performed *via* confocal microscopy (Nikon A1 S1 and Nikon C2+), imaging nuclei (Hoechst 34580), extracellular collagen (AF488) and BG4/iMab/γH2AX (AF594). For each antibody, identical acquisition settings were used for all samples.

All images were analysed using FIJI software (2.1.0) [30], by maximum intensity z-projections. For quantification of extracellular collagen, the AF488 channel had a binary threshold applied and the area with intensities above this threshold was measured. The number of cell nuclei in the image were measured from the Hoechst 34580 channel and the area of collagen per nuclei

Biomedical Optics EXPRESS

calculated. Foci per nuclei for γH2AX quantification was determined by first defining each cell nuclei identified from the Hoechst 34580 channel as a region of interest (ROI) then applying a binary threshold to the AF594 channel. For each ROI the 'analyse particles' function in FIJI was run on the thresholded AF594 channel, returning a count of foci per nuclei. Average fluorescence intensity per unit area for BG4 and iMab was measured by initially defining ROI corresponding to each nucleus identified *via* the Hoechst 34580 channel then using the 'measure' function in FIJI to measure the intensity of the AF594 channel and the area of the ROI, for each nucleus. Significance was determined in the form of p-value *via* Student's t-test that assumes the test statistic follows a normal distribution.

2.9. qPCR

Expression of the *COL1A1* gene was measured via quantitative polymerase chain reaction (qPCR). Cells were harvested with 1× TrypLE, RNA extracted and purified using Rneasy Mini Kit (Qiagen, 74106) then reverse transcribed using QuantiTect Reverse Transcription kit (Qiagen, 205311). The cDNA was then analysed using Quantinova SYBR Green PCR kit (Qiagen, 208056) on a Roche LightCycler 480 II using the *COL1A1* QuantiTect primer assay (Qiagen, QT00037793) with two housekeeping genes, *ACTB* and *GAPDH* (Qiagen, QT01680476, QT00079247). Changes in gene expression were determined via a comparative delta threshold cycle ($\Delta\Delta C_T$), normalising against the average of both housekeeping genes.

2.10. RNA-sequencing

Cells were harvested from two biological replicates with 1× TrypLE and RNA extracted and purified using Rneasy Mini Kit (Qiagen, 74106). Quantification and quality control was conducted via Nanodrop and Bioanalyser. RNA libraries were prepared using the TruSeq stranded total RNA with Ribo-Zero Human/Mouse/Rat library prep kit (Illumina) and sequenced (Illumina NovaSeq6000, 50×10^6 reads per sample, 150 bp PE) by Macrogen Oceania.

2.11. Analysis

Quality control of the fastq files was conducted using FastQC. Reads were aligned to the hg38 reference genome using STAR (version 2.5.1a) [31]. Reads were assigned to genes and counts generated using HTSeq (version 0.12.4) [32] using the Gencode gene annotation (Release 35 (GRCh38.p13)). Differential gene expression was analysed via EBSeq in R [33]. 255 genes were identified as differentially expressed at an FDR < 0.05. Gene set enrichment analysis was conducted on the genes ranked by $\log_2$FC × -$\log_{10}$(FDR) using the fgsea package [34]. Gene ontology enrichment analysis was conducted on significantly differentially expressed genes with FDR < 0.05 using the clusterProfiler package [35].

2.12. G4-iM grinder predictions

Potential sites of G4 and iM formation were predicted using the G4-iM Grinder function in R [36]. Predictions were run on the entirety of the hg38 genome, using a threshold score of 40 for pG4s and −40 for piMs. pG4/piM were identified within the region spanning from 2000 bp upstream to 1000 bp downstream of the transcription start site of the top 20 most significantly differentially expressed genes.

2.13. Thermal modelling

Finite difference time and frequency domain simulation methods were implemented using the COMSOL 5.4 Multiphysics package to model temperature fluctuations in the MMW-exposed cells. The physics module of Electromagnetic waves frequency domain was conjugated *via* the MMW heating Multiphysics interface to the Heat transfer module, which allowed transient estimation

Biomedical Optics EXPRESS

of sample heating and assessment of related dielectric losses. The raster-scanning pattern of the experimental MMW exposure was computationally accounted for using the Laminar Flow module. A single well of the 6-well plate was considered in the 3D model for simulation, which included a typical WR12 waveguide (length 10 mm) with a rounded flange output port to account for potential MMW reflections. Above the waveguide was a 1 mm air gap, a multi-well-plate plastic bottom (0.75 mm) and the layer of cells covered by saline (2 mm) enclosed in a MMW transparent, air-filled environment. 60 GHz, 100 mW MMW radiation was propagated through the waveguide without loss.

The distribution of the MMW power density along the vertical axis and at selected horizontal cross-sections was estimated from simulation using the relative permittivity (ε) and conductivity (σ) of the model materials. Typical values taken at ambient conditions were used for the polystyrene well ($\varepsilon = 2.4$, $\sigma = 0.003$) and the cell layer ($\varepsilon = 34$, $\sigma = 50$). The cell culture media was approximated as 300 mOsm saline solution and dielectric permittivity was defined from the Debye equation for a single relaxation time process, while the ionic conductivity was approximated by the equation for low saline concentrations (< 1 M) [37]. Properties of the polystyrene 6-well plate were measured using a commercial THz time-domain spectroscopy system (TeraPulse 4000; TeraView, Cambridge, UK) over a wide temperature range of 24–45°C. Density, viscosity, and heat capacity parameters were also introduced into the COMSOL model to improve the accuracy of simulation. Values of other materials used in the model were defined from the COMSOL libraries. A series of mesh sizes and parameter variations were used to confirm the absence of strong frequency-specific resonances.

2.14. Infrared imaging

MMW-exposed cells in 6-well plates were imaged using a Testo 885 infrared camera during the final raster cycle of the 5 h MMW exposure.

2.15. Thermal probe measurements

The temperature of media within the wells of the control and MMW-exposed cells in 6-well plates were measured *via* a fiber optic probe (Opsens) after 0, 2, 4, or 5 h MMW exposure.

3. Results and discussion

In this study we adopted a raster scan setup for MMW exposure to prevent focused heating effects as previous reports have shown the absorption of high power MMWs can cause thermal changes in the skin [12,15,38–42]. We confirmed via experimental measurements and computational modelling there was negligible associated heating ($\Delta T_{max} \sim +1.2$ °C) for the exposure time in our experimental setup (Supplement 1, Fig. S1). Additionally, we confirmed that the raster scanning motion and environment did not have an effect on collagen levels at the gene or protein level (Supplement 1, Fig. S1).

To examine the effect of MMWs on primary human fibroblasts at the cellular level we used immunocytochemistry to explore extracellular collagen, a common marker of fibroblast stimulation. Increased collagen deposition was observed following MMW exposure (5 h per day for 4 days; 46.8 J cm^{-2} d^{-1}, total dose 187.2 J cm^{-2}; Figs. 1(a) and 1(b)), with a corresponding increase in alignment of the extracellular collagen fibres (Fig. 1(c)). We further corroborated this at a transcriptional level using RT-qPCR which revealed that expression of *COL1A1* expression was both time- and dose-dependent, with a maximum 1.55-fold increase after 2 d (Fig. 1(d) and Supplement 1, Fig. S2). These elevated levels of *COL1A1* after 2 d drive the increase in extracellular collagen after 4 d as per the well-characterised delay of protein changes relative to mRNA changes [43,44]. Control experiments confirmed that *COL1A1* expression and collagen deposition by primary human fibroblasts was increased in response to TGF-β and unchanged where MMW exposure was absent (Supplement 1, Fig. S1) [45].

Biomedical Optics EXPRESS

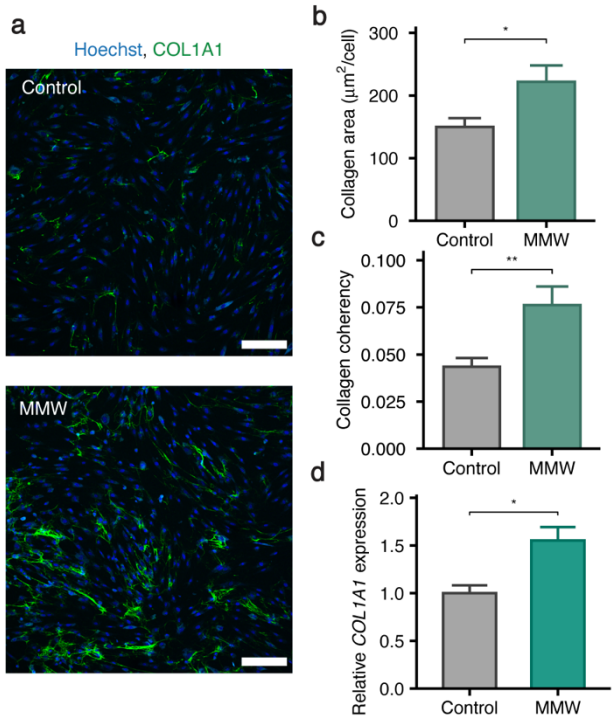

Fig. 1. MMWs induce a fibrotic response in primary human fibroblasts. (a) Representative confocal images of day 4 MMW exposed primary human fibroblasts using a COL1A1 specific antibody (green: COL1A1, blue: nuclei, Hoechst 34580; magnification: 10x; numerical aperture: 0.45; scale bar: 200 μm). (b) Quantification of extracellular collagen in control and MMW-exposed cells shows the area of collagen produced per cell (*$p < 0.05$, $n \geq 135$ cells per condition, 36 images). Data is represented as mean ± SEM. (c) Coherency of the extracellular collagen fibers in control and MMW-exposed cells. Coherency was measured from the alignment of collagen fibers in consistently sized regions of interest in confocal images. (**$p < 0.01$, $n = 72$ regions of interest per condition). Data is represented as mean ± SEM. (d) Relative expression of *COL1A1* mRNA after 2 d MMW exposure, determined via qPCR. Data is represented as mean ± SEM from three biological replicates (*$p < 0.05$, $n = 3$).

Biomedical Optics EXPRESS

Next, we investigated transcriptome-wide alterations to gene expression levels with RNA-seq as we show in Dataset 1 (Ref. [46]). Principal component analysis (PCA) revealed variations between control and MMW-exposed cells (5 h per day for 2 d; 46.8 J cm^{-2} d^{-1}, total dose 93.6 J cm^{-2}), representing the unique effect of MMWs on the transcriptome (Fig. 2(a)). Analysis of gene expression levels identified 255 significantly differentially expressed genes (DEGs) between control and MMW-exposed samples with a false discovery rate (FDR) < 0.05 across both biological replicates. Of these DEGs, 126 genes were upregulated and 129 genes were downregulated (Figs. 2(b) and (c)). The RNA-seq results identified a 1.46-fold increase in *COL1A1* gene expression, similar to qPCR and confirming the altered collagen deposition is driven by MMW-induced transcriptional modifications (Fig. 1(d)). Importantly, of the 255 MMW-induced DEGs, only 58 were also observed following TGF-β treatment (Fig. 2(d)), which had a total of 1162 DEGs across both biological replicates (Supplement 1, Fig. S3). The remaining 197 DEGs were unique to MMW-exposed cells and not significantly altered by TGF-β. Additionally, only 45% of genes that are over- or under-expressed with $|\log_2 FC| > 0.5$ in MMW-exposed cells are similarly up- or down-regulated by TGF-β treatment (Fig. 2(e)). Thus, most genes are differently affected by MMW and TGF-β treatments, indicating that the observed MMW-induced changes are different from the traditional cytokine-induced response.

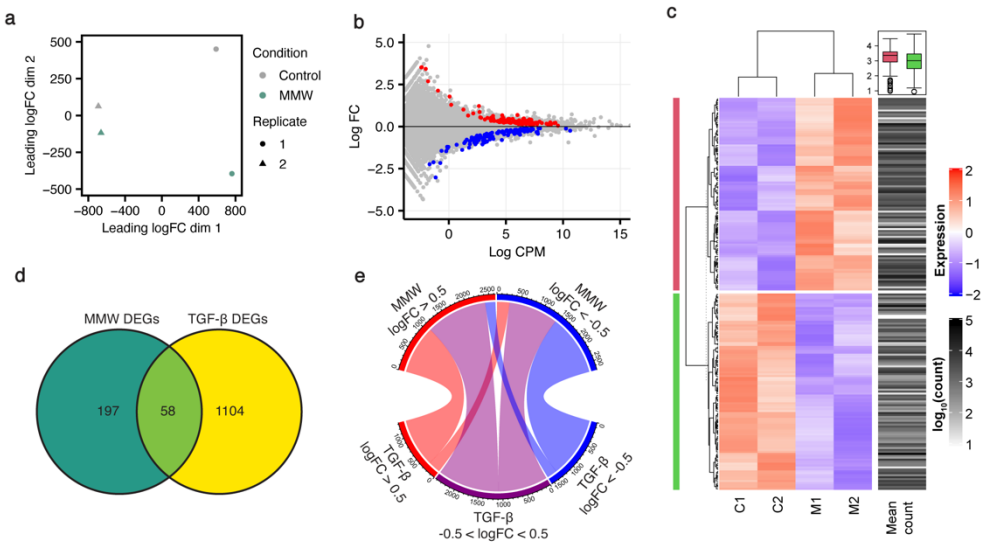

Fig. 2. MMWs cause unique transcriptomic modifications. (a) Principal component analysis (PCA) of RNA-seq data from untreated (control) and MMW-exposed primary human fibroblasts. Dots represent samples, with condition indicated by colour and biological replicate by shape. (b) MD plot reveals the log fold change and average abundance of each gene, with significantly differentially expressed (FDR < 0.05) genes shown in red (upregulated) and blue (downregulated). (c) Heatmap showing relative expression and abundance of the top 200 differentially expressed genes. Colour corresponds to the relative expression levels, while the intensity of the mean count column indicates the average abundance of the gene. The mean counts of MMW up- and down- regulated genes are shown by pink and green groupings in the boxplot. (d) Venn diagram of differentially expressed genes (DEGs) by MMW exposure and transforming growth factor beta (TGF-β) treatment. 58 genes are differentially expressed by MMWs and TGF-β. (e) Chord diagram of all genes with $|\log_2 FC| > 0.5$ in expression following 2 d MMW exposure. Genes are compared with their expression level in TGF-β treated cells, with $\log_2 FC > 0.5$ in red, $\log_2 FC < -0.5$ in blue and $-0.5 < \log_2 FC < 0.5$ in grey.

Biomedical Optics EXPRESS

While we have shown *via* thermometry that there are negligible bulk heating effects using our experimental set up, the potential for transitory localized heating to alter the temperature distribution at the cellular level remains and has previously been presented as a mechanism describing the interactions of electromagnetic radiation with cells [47]. However, the MMW-induced transcriptomic modifications identified *via* RNA-seq do not include the markers of a typical thermal response, suggesting that the effects do not arise as part of the cellular response to heating but as a consequence of MMW interactions with biomolecules, possibly through transient localized temperature fluctuations. Of note, only a single heat-shock related gene, *HSPA8*, is differentially expressed by MMW exposure, while the remaining 208 genes related to heat shock factor 1 (HSF1) activation, HSF1-dependent transactivation, cellular response to heat stress and regulation of HSF1-mediated heat shock response pathways, and the production of heat shock proteins are not differentially altered (Table S1).

Gene Set Enrichment Analysis (GSEA) and Gene Ontology (GO) analysis on the gene expression data identified numerous pathways that are differentially modified by MMW exposure (Fig. 3). In particular, many DNA- and cell cycle- associated pathways were identified as potentially altered by MMW exposure, including DNA replication, packaging, and conformational change, and S phase, M phase, and G2/M checkpoint processes. The disproportionate modification of genes related to these pathways suggests they are specifically altered by MMW exposure. Interestingly, cell cycle progression involves global chromatin restructuring and DNA replication, representing additional potential MMW-induced DNA modifications. GO analysis of the gene expression data for our positive control model of TGF-β treatment also identified numerous significant pathways of interest (Supplement 1, Fig. S3). In contrast to MMW exposure, no pathways associated with DNA structure or replication were altered. Rather, many pathways relating to the extracellular matrix, actin filaments and the cell-substrate junction are significantly modified, consistent with the increase in collagen deposition and *COL1A1* expression observed via immunocytochemistry and qPCR (Supplement 1, Fig. S1). The pathways affected by MMWs differ considerably from TGF-β treatment, representing unique interaction mechanisms and biological effects beyond altered collagen formation. Additionally, the pathways altered by MMWs are also unique compared to other electromagnetic frequencies. Previously, Hough *et al.* demonstrated that similarly high doses (44.3 J cm^{-2}) of intense broadband terahertz pulses (0.6 THz peak-power frequency, bandwidth of 1.8 THz FWTM) also modify gene expression in skin cells, however these genes are associated with cancer-related biological pathways [48,49]. The difference between the genes and pathways altered by MMW and terahertz exposure confirms that the biological interactions are frequency dependent, representing unique MMW effects.

MMW-induced transcriptomic modifications represent altered transcription of the affected genes, a process that involves complex interactions between DNA-binding proteins and genomic DNA sequences that are governed by sequence- and structure-specific interactions [50,51]. Several of the pathways associated with MMW-induced DEGs relate to DNA structural changes, including DNA conformational change, packaging, geometric change, and duplex unwinding, indicating MMWs may alter transcription at the DNA level. In particular, these pathways represent processes that are associated with DNA secondary structures, including G4s and iMs. Additionally, in previous *in vitro* studies of TGF-β-treated fibroblasts we have demonstrated that an increase in *COL1A1* gene expression and type 1 collagen protein levels are linked to changes in G4 formation [28]. Thus, we evaluated the effects of MMWs on G4 and iM formation in cells using the structure specific BG4 [52] and iMab [29] antibodies, respectively, as markers for genomic conformational alterations. Significant decreases in both DNA G4 and iM formation were observed following MMW exposure (Figs. 4(c) and (d)). Importantly, DNA G4s and iMs both functionally contribute to transcriptional regulation [25,26] and these structural changes have previously been associated with fibroblast stimulation [28]. We next tested if the observed changes in G4s and iMs were associated with DNA double-stranded breaks. Immunocytochemistry

Biomedical Optics EXPRESS

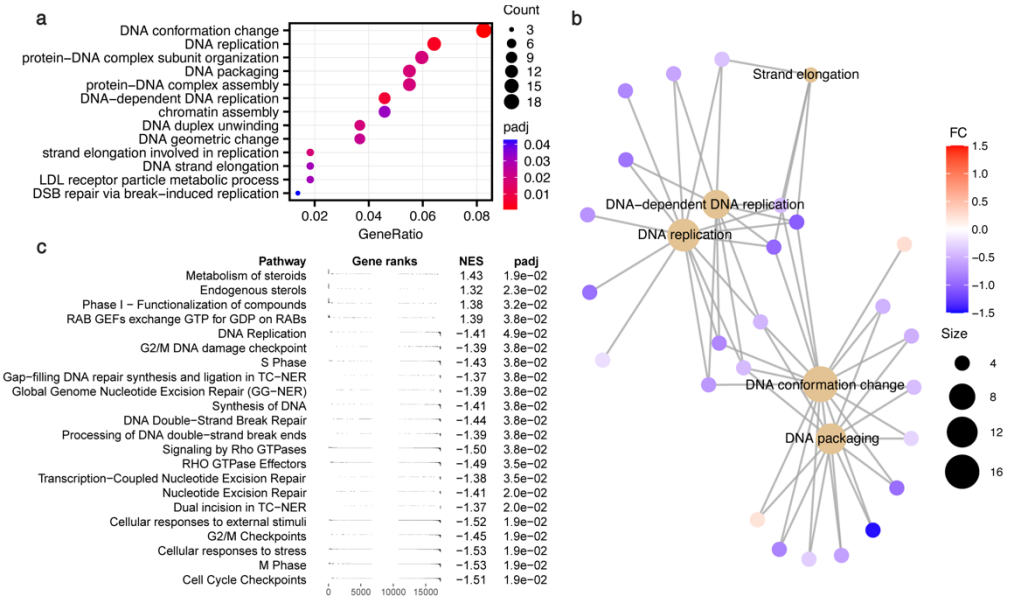

Fig. 3. Biological pathway modifications from RNA-seq data of 2 day MMW exposed cells. (a) Dot plot of gene ontology (GO) analysis of MMW differentially expressed genes plotted against gene ratio. Color indicates the adjusted p-value of the pathway and dot size corresponds to the number of DEGs in each pathway. (b) cnetplot of several pathways identified by GO identifies the DEGs associated with each pathway. The relative expression of each gene is represented by color, while size corresponds to the number of genes related to each pathway. (c) Gene set enrichment analysis (GSEA) identifies pathways by expression levels of relevant genes from RNA-seq of MMW-exposed cells. The distribution of genes associated with each pathway is indicated (gene ranks), as is the normalized enrichment score (NES) and adjusted p-value.

with a γH2AX-specific antibody revealed no change in the presence of phosphorylated histone variant H2AX, indicating that the MMW exposure did not induce DNA damage (Supplement 1, Fig. S4). To further investigate the link between MMW altered DNA secondary structures and the transcriptome, we utilised a G4 and iM prediction algorithm (G4-iM Grinder) [36] to investigate the propensity for the promoter regions of MMW-induced DEGs to form these secondary structures. Using a stringent threshold score of 40, we identified that of the top 20 DEGs, 16 contain at least one predicted G4- or iM- forming sequence (pG4 and piM, respectively) within the region spanning from 2000 bp upstream to 1000 bp downstream of the transcription start site (TSS), which includes distal, proximal, and downstream promoter regions that are integral in regulating transcription [53,54]. Of these top 20 DEGs, 7 are downregulated and 13 are upregulated, of which 6 and 10, respectively, contain pG4 or piM sites which potentially contribute to their transcriptional regulation (Fig. 4(e)). Many DEGs contain multiple G4/iM formation sites and the possibility for formation of both structures. Of note, CDV3, CAMSAP2, ITGAV, CLIC4, TSHZ2 all have a piM site less than 300 bp upstream of the TSS, while only CAMSAP2 has a pG4 in this region. Furthermore, these 20 genes are associated with biological pathways relevant to extracellular matrix components, such as collagen, and DNA structure, including focal adhesion (5/20), cell cycle arrest (3/20) and DNA conformational change (3/20), suggesting these G4 and iM structures are implicated in the biological responses to MMWs via modulation of gene expression levels (Table S2).

Biomedical Optics EXPRESS

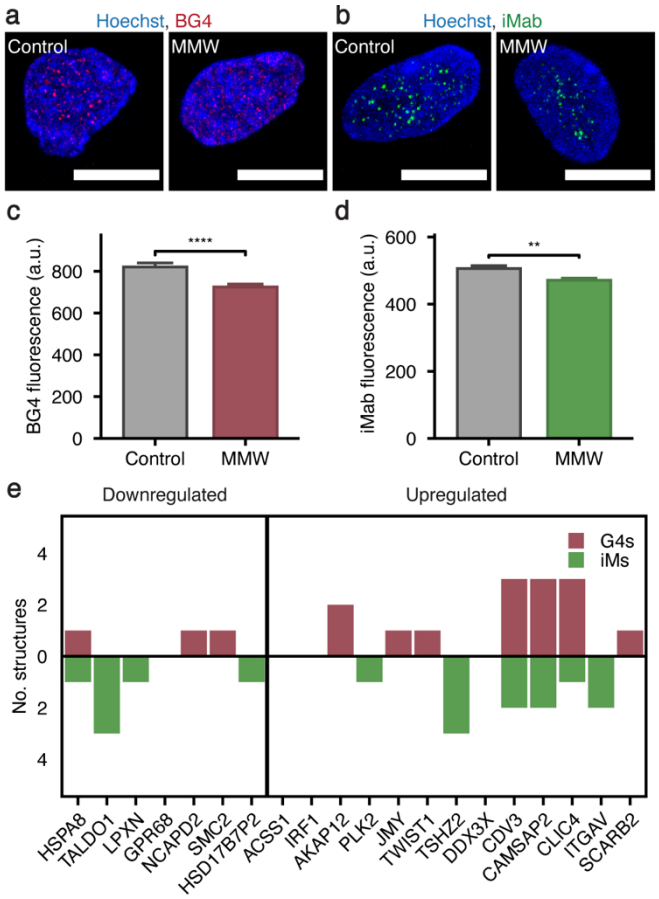

Fig. 4. G4 and iM populations are altered in MMW exposed cells. (a-b) Representative confocal images of nuclei stained with the G4 and iM structure specific antibodies scFv-BG4 and scFv-iMab, respectively (red: BG4, green: iMab, blue: nuclei, Hoechst 34580; magnification: 100x; numerical aperture: 1.4; scale bar: 10 µm. (c) The average fluorescence intensity/area of BG4 in the nuclei of control and MMW-exposed fibroblasts (****$p < 0.0001$, $n = 117$ nuclei). Data is represented as mean ± SEM. (d) The average fluorescence intensity/area of iMab in the nuclei of control and MMW-exposed fibroblasts (**$p < 0.01$, $n = 58$ nuclei). Data is represented as mean ± SEM. (e) Bar chart represents the propensity of potential G4 (red) and iM (green) sites identified by G4-iM Grinder in the promoter regions of the top 20 MMW differentially expressed genes.

Biomedical Optics EXPRESS

In this work we have correlated altered gene expression with genomic modifications and collagen production, describing a potential MMW interaction mechanism not associated with the typical cellular thermal response and the downstream effects. Previously, MMWs have been shown to induce a range of biological effects at the cellular level, including alterations to neuronal action potentials [12], membrane properties [13,14], and gene expression [15–19]. Of studies investigating the effects of MMWs on gene expression, most use either low power exposures and find minimal alterations [16–18], or very high powers, inducing significant heating and alterations of heat-shock related genes [15,19]. Compared to these high-power studies which used 75 mW cm^{-2} and 20 mW cm^{-2} power densities and caused temperatures to increase above 41 °C, we observed transcriptomic modifications after 2.6 mW cm^{-2} exposures without significant heating. Interestingly, Millenbaugh et al. also identified changes in several genes associated with collagen production, suggesting this is a biological process often affected by MMW exposure [19]. Together these results indicate a strong power and dose dependence of MMW-induced effects, representing an important avenue of future research to characterise MMW effects at biologically relevant exposure levels, such as at the limits recommended by the International Commission on Non-ionising Radiation Protection. Additionally, with a range of MMW frequencies proposed for implementation in modern communication technologies, the frequency dependence of these effects is an interesting area for future study.

In conclusion, our findings demonstrate that high dose MMWs can induce characteristic transcriptomic and genomic modifications in primary human fibroblasts that are not associated with a typical cellular thermal response. We show that MMW-induced changes at the transcriptome level are distinct from a traditional cytokine-induced transition, and that they may be associated with alterations in DNA structural dynamics. These changes represent unique interactions of MMWs with biological material and illustrate the importance of both power density and dose when determining safety margins for longer periods.

Funding. Australian Research Council; National Health and Medical Research Council.

Acknowledgments. We thank P. Schofield and D. U. Christ of Garvan Institute of Medical Research for providing the iMab scFv fragment. The authors acknowledge the facilities and the scientific and technical assistance of the Australian Microscopy & Microanalysis Research Facility at the Centre for Microscopy, Characterisation & Analysis, The University of Western Australia, a facility funded by the University, State and Commonwealth Governments. N. B. Lawler acknowledges the support of the Forrest Research Foundation. V. P. Wallace is supported by the Australian Research Council via a Future Fellowship (project number FT180100683) funded by the Australian Government.

Disclosures. The authors declare no conflicts of interest.

Data availability. Data underlying the results presented in this paper are available in Dataset 1, Ref. [46].

Supplemental document. See Supplement 1 for supporting content.

References

1. C. Park and T. S. Rappaport, "Short-range wireless communications for next-generation networks: UWB, 60 GHz millimeter-wave WPAN, and ZigBee," IEEE Wireless Commun. **14**(4), 70–78 (2007).
2. F. A. Dicandia and S. Genovesi, "Exploitation of triangular lattice arrays for improved spectral efficiency in massive MIMO 5G systems," IEEE Access **9**, 17530–17543 (2021).
3. S. K. Yong and C.-C. Chong, "An overview of multigigabit wireless through millimeter wave technology: potentials and technical challenges," J Wireless Com Network **2007**(1), 078907 (2006).
4. W. Hong, Z. H. Jiang, C. Yu, D. Hou, H. Wang, C. Guo, Y. Hu, L. Kuai, Y. Yu, Z. Jiang, Z. Chen, J. Chen, Z. Yu, J. Zhai, N. Zhang, L. Tian, F. Wu, G. Yang, Z.-C. Hao, and J. Y. Zhou, "The role of millimeter-wave technologies in 5G/6G wireless communications," IEEE J. Microw. **1**(1), 101–122 (2021).
5. W. Hong, Z. H. Jiang, C. Yu, J. Zhou, P. Chen, Z. Yu, H. Zhang, B. Yang, X. Pang, M. Jiang, Y. Cheng, M. K. T. Al-Nuaimi, Y. Zhang, J. Chen, and S. He, "Multibeam antenna technologies for 5G wireless communications," IEEE Trans. Antennas Propag. **65**(12), 6231–6249 (2017).
6. R. Appleby and R. N. Anderton, "Millimeter-wave and submillimeter-wave imaging for security and surveillance," Proc. IEEE **95**(8), 1683–1690 (2007).
7. P. Rosenkranz, "Shape of the 5 mm oxygen band in the atmosphere," IEEE Trans. Antennas Propag. **23**(4), 498–506 (1975).

Biomedical Optics EXPRESS

8. S. Singh, R. Mudumbai, and U. Madhow, "Interference analysis for highly directional 60-GHz mesh networks: the case for rethinking medium access control," IEEE/ACM Trans. Networking **19**(5), 1513–1527 (2011).
9. F. Giannetti, M. Luise, and R. Reggiannini, "Mobile and personal communications in the 60 GHz band: a survey," Wireless Personal Communications **10**(2), 207–243 (1998).
10. M.-O. Mattsson, O. Zeni, and M. Simkó, "Is there a biological basis for therapeutic applications of millimetre waves and THz waves?" J Infrared Milli Terahz Waves **39**(9), 863–878 (2018).
11. Y. Le Dréan, Y. S. Mahamoud, Y. Le Page, D. Habauzit, C. Le Quément, M. Zhadobov, and R. Sauleau, "State of knowledge on biological effects at 40–60 GHz," C. R. Phys. **14**(5), 402–411 (2013).
12. S. Romanenko, A. R. Harvey, L. Hool, S. Fan, and V. P. Wallace, "Millimeter wave radiation activates leech nociceptors via TRPV1-like receptor sensitization," Biophys. J. **116**(12), 2331–2345 (2019).
13. M. Zhadobov, R. Sauleau, V. Vie, M. Himdi, L. L. Coq, and D. Thouroude, "Interactions between 60-GHz millimeter waves and artificial biological membranes: dependence on radiation parameters," IEEE Trans. Microwave Theory Techn. **54**(6), 2534–2542 (2006).
14. A. Ramundo-Orlando, "Effects of millimeter waves radiation on cell membrane - a brief review," J Infrared Milli Terahz Waves **31**(12), 1400–1411 (2010).
15. D. Habauzit, C. L. Quément, M. Zhadobov, C. Martin, M. Aubry, R. Sauleau, and Y. L. Dréan, "Transcriptome analysis reveals the contribution of thermal and the specific effects in cellular response to millimeter wave exposure," PLoS ONE **9**(10), e109435 (2014).
16. C. L. Quément, C. N. Nicolaz, M. Zhadobov, F. Desmots, R. Sauleau, M. Aubry, D. Michel, and Y. L. Dréan, "Whole-genome expression analysis in primary human keratinocyte cell cultures exposed to 60 GHz radiation," Bioelectromagnetics **33**(2), 147–158 (2012).
17. C. N. Nicolaz, M. Zhadobov, F. Desmots, A. Ansart, R. Sauleau, D. Thouroude, D. Michel, and Y. L. Drean, "Study of narrow band millimeter-wave potential interactions with endoplasmic reticulum stress sensor genes," Bioelectromagnetics **30**(5), 365–373 (2009).
18. M. Zhadobov, R. Sauleau, L. L. Coq, L. Debure, D. Thouroude, D. Michel, and Y. L. Dréan, "Low-power millimeter wave radiations do not alter stress-sensitive gene expression of chaperone proteins," Bioelectromagnetics **28**(3), 188–196 (2007).
19. N. J. Millenbaugh, C. Roth, R. Sypniewska, V. Chan, J. S. Eggers, J. L. Kiel, R. V. Blystone, and P. A. Mason, "Gene expression changes in the skin of rats induced by prolonged 35 GHz millimeter-wave exposure," Radiat. Res. **169**(3), 288–300 (2008).
20. S. I. Alekseev, A. A. Radzievsky, M. K. Logani, and M. C. Ziskin, "Millimeter wave dosimetry of human skin," Bioelectromagnetics **29**(1), 65–70 (2008).
21. C. M. Alabaster, "Permittivity of human skin in millimetre wave band," Electron. Lett. **39**(21), 1521–1522 (2003).
22. T. A. Wynn, "Cellular and molecular mechanisms of fibrosis," J. Pathol. **214**(2), 199–210 (2008).
23. M. Simkó and M.-O. Mattsson, "5G wireless communication and health effects—a pragmatic review based on available studies regarding 6 to 100 GHz," IJERPH **16**(18), 3406 (2019).
24. International Commission on Non-Ionizing Radiation Protection (ICNIRP), "Guidelines for limiting exposure to electromagnetic fields (100 kHz to 300 GHz)," Health Physics **118**(5), 483–524 (2020).
25. R. Hänsel-Hertsch, M. Di Antonio, and S. Balasubramanian, "DNA G-quadruplexes in the human genome: detection, functions and therapeutic potential," Nat Rev Mol Cell Biol **18**(5), 279–284 (2017).
26. S. L. Brown and S. Kendrick, "The i-motif as a molecular target: more than a complementary DNA secondary structure," Pharmaceuticals **14**(2), 96 (2021).
27. E. L. Schneider and Y. Mitsui, "The relationship between in vitro cellular aging and in vivo human age," Proc. Natl. Acad. Sci. U.S.A. **73**(10), 3584–3588 (1976).
28. P. Toshniwal, M. Nguyen, A. Guédin, H. Viola, D. Ho, Y. Kim, U. Bhatt, C. S. Bond, L. Hool, L. H. Hurley, J.-L. Mergny, M. Fear, F. Wood, S. K. Iyer, and N. M. Smith, "TGF-β-induced fibrotic stress increases G-quadruplex formation in human fibroblasts," FEBS Lett. **593**(22), 3149–3161 (2019).
29. M. Zeraati, D. B. Langley, P. Schofield, A. L. Moye, R. Rouet, W. E. Hughes, T. M. Bryan, M. E. Dinger, and D. Christ, "I-motif DNA structures are formed in the nuclei of human cells," Nature Chem **10**(6), 631–637 (2018).
30. J. Schindelin, I. Arganda-Carreras, E. Frise, V. Kaynig, M. Longair, T. Pietzsch, S. Preibisch, C. Rueden, S. Saalfeld, B. Schmid, J.-Y. Tinevez, D. J. White, V. Hartenstein, K. Eliceiri, P. Tomancak, and A. Cardona, "Fiji: an open-source platform for biological-image analysis," Nat Methods **9**(7), 676–682 (2012).
31. A. Dobin, C. A. Davis, F. Schlesinger, J. Drenkow, C. Zaleski, S. Jha, P. Batut, M. Chaisson, and T. R. Gingeras, "STAR: ultrafast universal RNA-seq aligner," Bioinformatics **29**(1), 15–21 (2013).
32. S. Anders, P. T. Pyl, and W. Huber, "HTSeq—a Python framework to work with high-throughput sequencing data," Bioinformatics **31**(2), 166–169 (2015).
33. N. Leng, J. A. Dawson, J. A. Thomson, V. Ruotti, A. I. Rissman, B. M. G. Smits, J. D. Haag, M. N. Gould, R. M. Stewart, and C. Kendziorski, "EBSeq: an empirical Bayes hierarchical model for inference in RNA-seq experiments," Bioinformatics **29**(8), 1035–1043 (2013).
34. G. Korotkevich, V. Sukhov, and A. Sergushichev, "Fast gene set enrichment analysis," bioRxiv, 060012 (2019).
35. G. Yu, L.-G. Wang, Y. Han, and Q.-Y. He, "clusterProfiler: an R package for comparing biological themes among gene clusters," OMICS: A Journal of Integrative Biology **16**(5), 284–287 (2012).

Biomedical Optics EXPRESS

36. E. Belmonte-Reche and J. C. Morales, "G4-iM Grinder: when size and frequency matter. G-Quadruplex, i-Motif and higher order structure search and analysis tool," NAR Genomics and Bioinformatics **2**(1), lqz005 (2020).
37. A. Peyman, C. Gabriel, and E. H. Grant, "Complex permittivity of sodium chloride solutions at microwave frequencies," Bioelectromagnetics **28**(4), 264–274 (2007).
38. A. Radzievsky, O. Gordiienko, A. Cowan, S. I. Alekseev, and M. C. Ziskin, "Millimeter-wave-induced hypoalgesia in mice: dependence on type of experimental pain," IEEE Trans. Plasma Sci. **32**(4), 1634–1643 (2004).
39. S. Romanenko, R. Begley, A. R. Harvey, L. Hool, and V. P. Wallace, "The interaction between electromagnetic fields at megahertz, gigahertz and terahertz frequencies with cells, tissues and organisms: risks and potential," J. R. Soc. Interface. **14**(137), 20170585 (2017).
40. M. Zhadobov, N. Chahat, R. Sauleau, C. L. Quement, and Y. L. Drean, "Millimeter-wave interactions with the human body: state of knowledge and recent advances," Int. j. microw. wirel. technol. **3**(2), 237–247 (2011).
41. S. I. Alekseev, O. V. Gordiienko, A. A. Radzievsky, and M. C. Ziskin, "Millimeter wave effects on electrical responses of the sural nerve in vivo," Bioelectromagnetics **31**(3), 180 (2009).
42. C. L. Quément, C. N. Nicolaz, D. Habauzit, M. Zhadobov, R. Sauleau, and Y. L. Dréan, "Impact of 60-GHz millimeter waves and corresponding heat effect on endoplasmic reticulum stress sensor gene expression," Bioelectromagnetics **35**(6), 444–451 (2014).
43. M. Jovanovic, M. S. Rooney, P. Mertins, D. Przybylski, N. Chevrier, R. Satija, E. H. Rodriguez, A. P. Fields, S. Schwartz, R. Raychowdhury, M. R. Mumbach, T. Eisenhaure, M. Rabani, D. Gennert, D. Lu, T. Delorey, J. S. Weissman, S. A. Carr, N. Hacohen, and A. Regev, "Dynamic profiling of the protein life cycle in response to pathogens," Science **347**(6226), 1259038 (2015).
44. Y. Liu, A. Beyer, and R. Aebersold, "On the dependency of cellular protein levels on mRNA abundance," Cell **165**(3), 535–550 (2016).
45. C. Chen, Y. Peng, Z. Wang, P. Fish, J. Kaar, R. Koepsel, A. Russell, R. Lareu, and M. Raghunath, "The Scar-in-a-Jar: studying potential antifibrotic compounds from the epigenetic to extracellular level in a single well," Br J Pharmacol **158**(5), 1196–1209 (2009).
46. N. B. Lawler, C. W. Evans, S. Romanenko, N. Chaudhari, M. Fear, F. Wood, N. M. Smith, V. P. Wallace, and K. S. Iyer, "Raw RNA-seq data, accession number GSE197295," NCBI's Gene Expression Omnibus, 2022, https://www.ncbi.nlm.nih.gov/geo/query/acc.cgi?acc=GSE197295.
47. A. G. Markelz and D. M. Mittleman, "Perspective on terahertz applications in bioscience and biotechnology," ACS Photonics (2022).
48. C. M. Hough, D. N. Purschke, C. Huang, L. V. Titova, O. V. Kovalchuk, B. J. Warkentin, and F. A. Hegmann, "Intense terahertz pulses inhibit Ras signaling and other cancer-associated signaling pathways in human skin tissue models," J. Phys. Photonics **3**(3), 034004 (2021).
49. C. M. Hough, D. N. Purschke, C. Huang, L. V. Titova, O. Kovalchuk, B. J. Warkentin, and F. A. Hegmann, "Topology-based prediction of pathway dysregulation induced by intense terahertz pulses in human skin tissue models," J. Infrared Milli. Terahz. Waves **39**(9), 887–898 (2018).
50. X. Zhang, J. Spiegel, S. Martínez Cuesta, S. Adhikari, and S. Balasubramanian, "Chemical profiling of DNA G-quadruplex-interacting proteins in live cells," Nat. Chem. **13**(7), 626–633 (2021).
51. P. J. Mitchell and R. Tjian, "Transcriptional regulation in mammalian cells by sequence-specific DNA binding proteins," Science **245**(4916), 371–378 (1989).
52. G. Biffi, D. Tannahill, J. McCafferty, and S. Balasubramanian, "Quantitative visualization of DNA G-quadruplex structures in human cells," Nature Chem **5**(3), 182–186 (2013).
53. R. Hänsel-Hertsch, D. Beraldi, S. V. Lensing, G. Marsico, K. Zyner, A. Parry, M. Di Antonio, J. Pike, H. Kimura, M. Narita, D. Tannahill, and S. Balasubramanian, "G-quadruplex structures mark human regulatory chromatin," Nat. Genet. **48**(10), 1267–1272 (2016).
54. W. Zhou, K. Suntharalingam, N. J. Brand, P. J. R. Barton, R. Vilar, and L. Ying, "Possible regulatory roles of promoter G-quadruplexes in cardiac function-related genes–human TNIC as a model," PLoS ONE **8**(1), e53137 (2013).